

EVALUATION OF Ω_M AND H_0 FROM ISOTROPIC 2PCF BAO STUDIES

JOEL S. JAYSON
P.O. Box 34
Brooklyn, N.Y 11235, USA
August 21, 2017

ABSTRACT

We have extracted weighted mean values of $\bar{\Omega}_{mw} = 0.296 \pm 0.008$ and $\bar{H}_{0w} = 68.7 \pm 0.55$ km s⁻¹Mpc⁻¹ from ten baryon acoustic oscillation (BAO) data sets, found in eight isotropic two point correlation function (2PCF) studies. Those results were obtained using fit-lines to CMB compatible solutions, but are independent of any particular CMB parameter set. Two central assumptions were employed. The first was a Λ CDM cosmology with $\Omega_K \simeq 0$ and a dark energy equation of state with $w \simeq -1$. Second, effects that perturb the BAO correlation function, $\xi(r)$, peak position at its co-moving radius of ~ 150 Mpc, were taken as constant over the small range that the peak is shifted from its fiducial to data position. Those perturbations include non-linearities, galaxy biasing and redshift distortion. That second assumption enables an accurate description of the 2PCF peak shift using a basic format, the Fourier transform of the matter power spectrum modified with the conventional no-wiggle term. The computed correlation function peak location, r_p , depends upon the damping parameter, k^* . We have performed computations with two k^* values that give widely disparate r_p values, yet find negligible effect on the outcomes. Additional to the parameter evaluations, we demonstrate that contrary to widespread usage, $D_V(z)/r_d \neq \alpha D_{Vf}(z)/r_{df}$. Here, $D_V(z)$ is the volume averaged distance, r_d is the acoustic sound horizon at the baryon drag epoch, the subscript, f , refers to fiducial values, and α is the correlation function peak shift-parameter.

Subject headings: cosmological parameters – early Universe – large-scale structure of Universe – cosmic background radiation

1. INTRODUCTION

Satellite expeditions conducted by NASA's Wilkinson Microwave Anisotropy Probe (*WMAP*) (Hinshaw et al. 2013) and ESA's *Planck* mission (*Planck* 2015 results XIII 2016), and the earth-bound, high altitude and high resolution observations conducted by the Atacama Cosmology Telescope (*ACT*) (Dunkley et al. 2013; Das et al. 2014) and the South Pole Telescope (*SPT*) (Story et al. 2013; George et al. 2015) have yielded an abundance of precise cosmic microwave background (CMB) data.

Three major initiatives have matured in parallel with the advanced CMB studies and complement that effort. Reliable super novae Ia (SNe Ia) measurements now number in the many hundreds (Suzuki et al. 2012; Betoule et al. 2014) leading to an independent assessment of cosmological parameters. Baryon acoustic oscillations (BAO) (Peebles & Yu 1970; Eisenstein et al. 1998b; Seo & Eisenstein 2003; Eisenstein et al. 2005; Cole et al. 2005; Percival et al. 2007), the other shoe that dropped after recombination, during the drag epoch, have been observed at several values of redshift, z . Analyses of large collections of galaxies have revealed correlations on the scale of the acoustic horizon, r_d , at the time of baryon photon decoupling. This in turn has ushered in an independent means of determining cosmic distances. (See Bassett & Hlozek (2010) and Aubourg et al. (2015) and references therein for an overview of results). Finally, the Hubble constant, first defined and measured close to nine decades ago (Hubble 1929), has been measured with increased exactitude (Riess et al. 2011; Freedman et al.

2012), and a recent publication details a measurement with an uncertainty of less than 2.5 per cent (Riess et al. 2016). The Hubble constant determinations of $H_0 \sim 73$ km s⁻¹Mpc⁻¹ at low redshift are persistently in tension with those ascertained from CMB measurements. The standard Λ CDM model explicitly assumes a homogeneous universe. Possibly, the violation of that assumption in the local vicinity explains the H_0 deviation (Bolejko, C el erier & Krasi nski 2011; Clarkson 2012).

Though tensions exist between parameter values extracted from the major initiatives, on the whole the Λ CDM concordance model that has emerged stands in solid agreement with the conclusions that were reached towards the close of the past century by two teams (Riess et al. 1998; Perlmutter et al. 1999) using SNe Ia observations. Those observations led to the inference that in recent times the Universe has begun to expand at an accelerated rate, that acceleration driven by a dark energy component that comprises about 70 per cent of the total matter-energy content. [See review, Weinberg et al. (2013)].

We focus herein on selected findings of the BAO initiative. At the drag epoch an overdense sphere of baryons was left behind around each of the randomly spaced overdensities with a comoving radius, r_d , of approximately 150 Mpc. This shell interacted gravitationally with the central CDM, and within about 500 Myrs the distribution of the CDM and baryonic fractions equilibrated (Eisenstein et al. 2007b). As matter coalesced into galaxies and clusters, the impression of the overdensities remained, offering the possibility of statistically recovering the acoustic scale, and hence a standard ruler. Because of its immense size, the effect of non-linearities

on the recovered feature is slight.

Since the first successful detections (Eisenstein et al. 2005; Cole et al. 2005) a steady stream of studies has followed, making good use of various galaxy surveys, e.g., the 2dF Galaxy Redshift Survey (2dF-GRS) (Colless et al. 2003), the WiggleZ Dark Energy Survey (Drinkwater et al. 2010), and a succession of Sloan Digital Sky Survey (SDSS) data releases (York et al. 2000). Data analyses employ either the modified matter power spectrum or its Fourier transform, the two point correlation function (2PCF), or both. The number of probed galaxies in a given study varies appreciably. Eisenstein et al. (2005) conducted their study with a spectroscopic sample of $\sim 47,000$ luminous red galaxies, while more recently Alam et al. (2016) have probed $\sim 1,200,000$ galaxies distributed over three overlapping redshift bins from the SDSS-III Baryon Oscillation Spectroscopic Survey (BOSS), Data Release 12 (Reid et al. 2016). The early studies, with limited numbers, obtained monopole/isotropic results. More recent investigations have additionally performed anisotropic analyses, evaluating both D_M , the comoving angular diameter distance, and $H(z)$, the Hubble constant at redshift z .

BAO measurements strive to use the acoustic scale over a range of redshifts to evaluate distances, the extent of spatial curvature, Ω_K , and the deviation of the dark energy equation of state from $w = -1$. At this juncture, precise CMB measurements have restricted any deviation from flatness to $|\Omega_K| < 0.005$, and combined CMB and SNe Ia measurements constrain w to -1.006 ± 0.045 (*Planck* 2015 results XIII 2016). Throughout this paper we rely on those restrictions to analyze BAO results over a range of CMB study compatible cosmologies.

Within the array of BAO investigations, we specifically concentrate on isotropic 2PCF studies. In doing so we make one further assumption. Though non-linearities are not a major concern at the large scale of r_d , they do have some effect on the BAO correlation function peak location, r_p , as do redshift distortions and galaxy biasing (Guzik, Bernstein & Smith 2007; Smith, Scoccimarro & Sheth 2008; Crocce & Scoccimarro 2008). These are of importance in determining the absolute acoustic scale. In this work, rather than focusing on that absolute scale we concentrate on the shift of the correlation function peak from a fiducial position to the position determined by the data. That shift, defined by a parameter, α , is usually small, a few per cent at most. We assume that over that limited range, to first order, the magnitude of the peak location perturbations does not change. Hence, regardless of procedures that were adopted in a specific work to account for those perturbations, we are able to work solely with the Fourier transform of the modified matter power spectrum, incorporating the no-wiggle form of Eisenstein & Hu (1998a, 1999) to account for the non-linearities at small scales.

We first derive r_p over a range of CMB compatible solutions, mapping Ω_m and H_0 as a function of r_p . Unlike fits to CMB TT power spectra curves for different CMB compatible solutions, the Ω_m and H_0 pairs are readily differentiated in the r_p mapping. Thus, the Ω_m , H_0 CMB degeneracy can be broken, computing r_p from BAO studies by using their fiducial cosmologies and derived values of α , and then reading the Ω_m and H_0 pair values from

the mapping of the CMB compatible solutions.

2PCF investigations widely apply a stated equality between $D_V(z)/r_d$ and $\alpha D_{Vf}(z)/r_{df}$ where $D_V(z)$ is the volume averaged distance construct introduced by Eisenstein et al. (2005),

$$D_V(z) = \left(D_M^2(z) \frac{cz}{H(z)} \right)^{1/3}. \quad (1)$$

The function $D_V(z)$ combines two parts of an angular distance and one part of a quantity designed to compensate for the distortion of radial distance in redshift space. It is universally used in isotropic BAO studies, where the derived angle characterizing the BAO correlation feature is given by $r_d/D_V(z)$, and most often by its reciprocal, $D_V(z)/r_d$. The additional subscript, f refers to the value of the fiducial cosmology and α is the factor, referred to above, by which the BAO correlation peak has been shifted from the position of the fiducial cosmology to that extracted from the data. ($\alpha > 1$ shifts the peak to a smaller radius.) We demonstrate that the presumed equality between the fiducial ratio times α and the derived ratio is incorrect.

In Section 2, in preparation for an analysis of BAO isotropic studies, we calculate the 2PCF for CMB compatible cosmologies and derive simple relationships between Ω_m , H_0 , the fiducial peak position, r_{pf} and the peak shift parameter, α . Section 3 presents a number of isotropic 2PCF studies and derives weighted mean values of Ω_m and H_0 from that body of work. In Section 4 we demonstrate that $D_V(z)/r_d \neq \alpha D_{Vf}(z)/r_{df}$. Our conclusions are set forth in Section 5.

2. CMB COMPATIBLE BAO SOLUTIONS

2.1. CMB Compatible Cosmologies

Considering that we assume CMB “compatible cosmologies” throughout, we begin by defining what is meant by that term. CMB TT power spectra curves that represent two widely differing Ω_m and H_0 pair values are plotted in Figure 1a. As indicated in the figure caption the fit parameters for the plots are found in Calabrese et al. (2017) (*Planck*) and in Hinshaw et al. (2013) (*WMAP9*). The designation, *WMAP9*+eCMB (“extended CMB”), refers to *WMAP9* data that has been supplemented with both *ACT* and *SPT* data at the higher multipoles. The CAMB software package (Lewis et al. 2000),¹ was used to generate the TT power spectra curves. Without referral to the residual plot of Figure 1b it is difficult to make out any significant difference between the two spectra. Though the CMB data is precise, there is a near degeneracy between Ω_m and H_0 that yields similar spectra for different pair values. As will be demonstrated, under these circumstances, Ω_m and H_0 are tied together in a strict relationship. It is that family of spectra that we refer to as CMB “compatible cosmologies.”

The relative amplitude of the CMB TT spectrum damping tail relates directly to the mass fraction, Ω_m , the higher the mass fraction the greater the amplitude of the tail relative to the power spectrum peak value (Hu & Dodelson 2002). Conversely, a relatively low

¹ Our calculations were derived from NASA’s online Lambda utility at <http://lambda.gsfc.nasa.gov>.

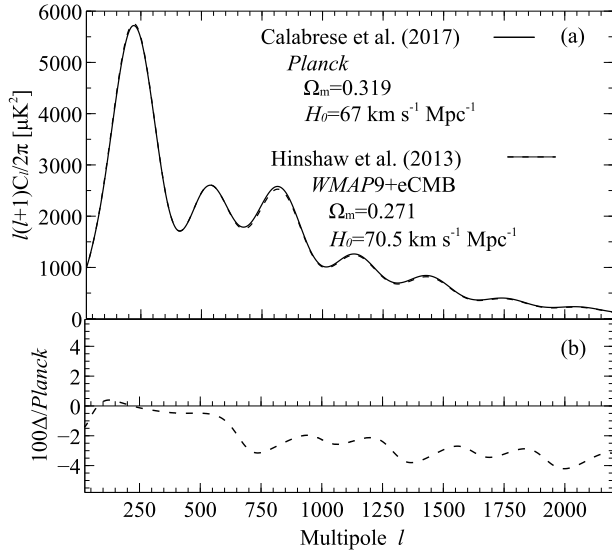


FIG. 1.— a) CMB TT power spectra comparing data from Calabrese et al. (2017), *Planck*, given in Table 1 and data from Hinshaw et al. (2013) for a *WMAP9*+eCMB fit. The minimum plotted value of the abscissa is $l=25$. Cosmic variance is increasingly significant below that point. The Hinshaw et al. (2013) spectrum has been multiplied by 0.9936, setting the two spectra amplitudes equal at the first peak. The differences between the two curves are barely perceptible on this scale. b) The fractional residuals, 100 times the difference between the *WMAP9*+eCMB and *Planck* data divided by the *Planck* data, illustrating how the damped tail has a lower amplitude for CMB solutions with lower values of Ω_m and higher values of H_0 .

damping tail is indicative of a higher value of H_0 . The term “damping tail” derives from Silk damping (Silk 1968), which occurred during the recombination epoch, when photon diffusion attenuated the acoustic oscillation amplitude at smaller angular scales.

WMAP preceded *Planck* and had a lower resolution, its maximum effective multipole was ~ 1000 . In the analysis of their nine-year data (Hinshaw et al. 2013), *WMAP9* appended the high resolution *ACT* and *SPT* data, which include TT multipoles well beyond the *WMAP9* range (the previously defined eCMB) allowing a comparison with *Planck*. *Planck* and *WMAP9* data are in good agreement through multipole 1000 (see fig. 48 of *Planck* 2015 results XI (2016)), although the same is not true for *Planck* and *WMAP9*+eCMB, or +*ACT*, or +*SPT*, where the *ACT* and *SPT* data draw the *WMAP9*+ curves below the *Planck* curve, as seen for *WMAP9*+eCMB in Figure 1b.

2.2. Determination of 2PCF Peak Positions

Since the co-moving radius of the BAO acoustic feature is ~ 150 Mpc, this large size has led to the feature being, on the whole, impervious to the nonlinearities introduced by the clustering of matter after recombination. Nonetheless, non-linear evolution, scale dependent galaxy biasing and red shift distortion do have an effect on the location of the correlation function peak (Guzik et al. 2007; Smith et al. 2008; Crocce & Scoccimarro 2008).

However, we do not require the absolute position of the BAO feature peak. Rather, we are looking at differences. We assume that to first order those differences are unaffected by the mechanisms that alter the absolute

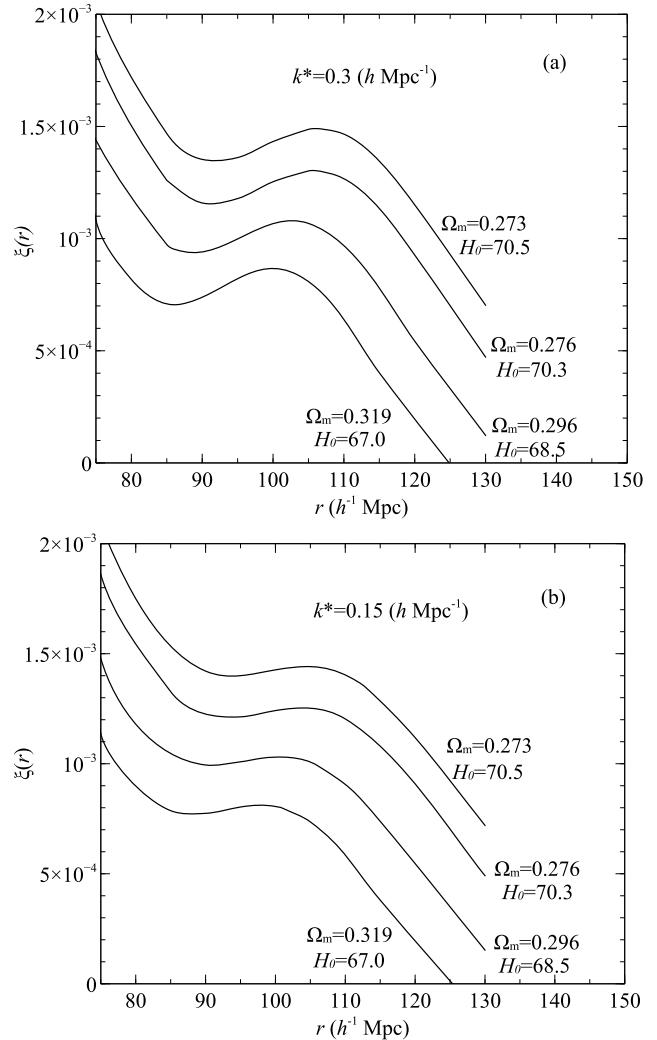


FIG. 2.— Correlation functions in real space for four sets of parameters that satisfy the CMB observations of *Planck* data, and of *ACT*, *SPT* and *ACT* + *SPT* data in combination with *WMAP9* from Calabrese et al. (2017) (see Table 1 for parameter values). The curves have been computed for a redshift, $z = 0.35$. (The peak locations are independent of redshift). Three plots have been offset vertically from that of the $\Omega_m = 0.319$, $H_0 = 67.0$ km s $^{-1}$ Mpc $^{-1}$ solution for ease of viewing. The ordinate axis scale refers to the $\Omega_m = 0.319$, $H_0 = 67.0$ curve. The dimensionless parameter h (in the units for r , h^{-1} Mpc) is used to define the Hubble constant, $H_0 = 100h$ km s $^{-1}$ Mpc $^{-1}$. (a) Curves computed using a value of $k^* = 0.3$ h Mpc $^{-1}$ in Eq. 2. (b) Same as (a) except that $k^* = 0.15$ h Mpc $^{-1}$.

position of the peak. Using that assumption, we evaluate the 2PCF without introducing corrections for the peak position perturbations. The CAMB software package generates the matter power spectrum, $P^{\text{lin}}(k)$, required for evaluating the correlation function. Eisenstein & Hu (1998a, 1999) introduced a baryon-free spectrum, “no-wiggle,” $P^{\text{nw}}(k)$ that when combined with $P^{\text{lin}}(k)$ provides a power spectrum that accounts for small scale nonlinearities by diminishing the higher order oscillations. With the inclusion of the no-wiggle term, the modified matter power spectrum, $p^{\text{mod}}(k)$, takes the form,

$$P^{\text{mod}}(k) = P^{\text{nw}}(k) + [P^{\text{lin}}(k) - P^{\text{nw}}(k)]e^{[-(k/k^*)^2/2]} \quad (2)$$

To obtain the correlation function in real space we take the Fourier transform of Equation (2) (Sánchez et al.

TABLE 1
 CMB PARAMETER SETS

| $\Omega_b h^2$ | $\Omega_c h^2$ | $10^9 \Delta_R^2$ | n_s | τ | h | Ω_m | Ref. |
|-----------------|----------------|-------------------|---------------|-------------|-------------|-------------|------|
| 0.02217±0.00021 | 0.1205±0.0021 | 2.14±0.04 | 0.9625±0.0056 | 0.064±0.01 | 0.670±0.009 | 0.319±0.013 | 1 |
| 0.02205±0.00028 | 0.1199±0.0027 | 2.20±0.06 | 0.9603±0.0073 | 0.089±0.013 | 0.673±0.012 | 0.315±0.017 | 2 |
| 0.02226±0.00023 | 0.1186±0.0020 | 2.14±0.06 | 0.9677±0.006 | 0.066±0.016 | 0.678±0.009 | 0.308±0.012 | 3 |
| 0.02243±0.00040 | 0.1156±0.0043 | 2.08±0.05 | 0.966±0.01 | 0.06±0.009 | 0.685±0.02 | 0.296±0.025 | 4 |
| 0.02242±0.00032 | 0.1134±0.0036 | 2.06±0.04 | 0.9638±0.0087 | 0.058±0.009 | 0.703±0.016 | 0.276±0.019 | 5 |
| 0.02223±0.00033 | 0.1126±0.0036 | 2.05±0.04 | 0.9610±0.0089 | 0.057±0.009 | 0.705±0.016 | 0.273±0.019 | 6 |

NOTE. — The neutrino mass, $\Sigma m_\nu = 0.06$ eV for all data sets. Ω_b is the baryon mass fraction, Ω_c the cold dark matter fraction, Δ_R^2 is the CMB amplitude term. The scalar spectral index is denoted by n_s and the reionization optical depth by τ . Calabrese et al. (2017), *Planck*, reference (1) refit the data from *Planck* 2015 results XIII (2016), reference (3). The differences in the Ω_m , h pair values is indicative of the Ω_m , h pair degeneracy in CMB TT spectra parameter evaluations.

REFERENCES. — (1) Calabrese et al. (2017), *Planck*; (2) *Planck* 2013 results XVI (2014); (3) *Planck* 2015 results XIII (2016); (4) Calabrese et al. (2017), *WMAP9+ACT*; (5) Calabrese et al. (2017), *WMAP9+eCMB*; (6) Calabrese et al. (2017), *WMAP9+SPT*

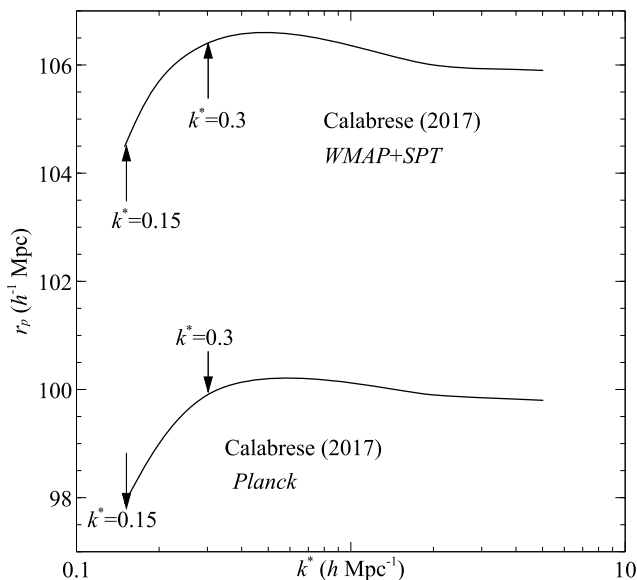


FIG. 3.— Peak values of $\xi(r)$ plotted for two CMB solutions as a function of the value of the damping factor, k^* used in Equation (2). Specific parameter values are listed in Table 1. Two sets of computations are performed in this paper, with $k^* = 0.15$ h Mpc^{-1} , and with $k^* = 0.3$ h Mpc^{-1} , to test whether the significant difference in their derived r_p values affects the results.

2008),

$$\xi(r) = \frac{1}{2\pi^2} \int_0^\infty dk k^2 P^{\text{mod}}(k) j_0(kr) e^{-k^2 a^2}. \quad (3)$$

Here, a^2 is a damping factor that has been introduced to regulate convergence of the numerical integration at higher values of k where the zero order spherical Bessel function, $j_0(kr)$ undergoes rapid oscillation. We set its value to 0.6 h^{-2} Mpc^2 , which ensures that it does not interfere with the determination of r_p .

Figure 2 depicts a series of correlation functions, each calculated using a set of cosmological parameters that satisfies CMB observations. The correlation function peak location, r_p , is dependent upon the value of the $P^{\text{mod}}(k)$ damping parameter, k^* . In Figure 2a, $k^* = 0.3$ h Mpc^{-1} , while in Figure 2 its value is 0.15 h Mpc^{-1} . Table 1 provides the relevant parameter values for six CMB data sets, four of which were used to derive the $\xi(r)$ curves of Figure 2.

In Figure 3, r_p is plotted as a function of k^* for the two cosmologies provided in Table 1 with the largest spread

in Ω_m and H_0 values. The choice of $k^* = 0.3$ and 0.15 h Mpc^{-1} for our computations was driven by the significant differences in r_p those values returned, and facilitates a rigorous test regarding the effect of k^* choice on outcomes. In Figures. 4a and 4b we have taken the correlation function peak results from Figure 2, along with computed r_p outcomes for the other two data sets of Table 1, and have derived fitted lines for the Table 1 Ω_m and H_0 values. A total of eleven pairs of Ω_m and H_0 taken from CMB studies and analyses, as referenced in the figure caption, are plotted in Figure 4 against $\xi(r)$ peak locations. The data sets from Table 1 were derived in the referenced works assuming the minimum neutrino mass, $\Sigma m_\nu = 0.06$ eV. The other five data sets had not incorporated a neutrino mass and we have not included them in computing the least-squares fits. Figure 4 data points (1) through (3) represent *Planck* derived quantities. At the other extreme, data point (11) was obtained from *WMAP3*. At an $\Omega_m = 0.238$ value, it is an outlier for *WMAP* for which their other data releases *WMAP1*, 5, 7 and 9 produced values of 0.27, 0.273, 0.272 and 0.279 respectively. Regardless, what is noteworthy from our viewpoint is that the *WMAP3* data point falls close to the fit lines.

In the following section we employ the fit-line formulas, using the identity $r_p \equiv r_{pf}/\alpha$. For $k^* = 0.3$ h Mpc^{-1} ,

$$H_0 = 11.8994 + 0.5513 \frac{r_{pf}}{\alpha} (\pm 0.080) \text{ km s}^{-1} \text{Mpc}^{-1} \quad (4)$$

$$\Omega_m = 1.0363 - 0.00718 \frac{r_{pf}}{\alpha} (\pm 0.0026) \quad (5)$$

and for $k^* = 0.15$ h Mpc^{-1} ,

$$H_0 = 13.6095 + 0.5453 \frac{r_{pf}}{\alpha} (\pm 0.12) \text{ km s}^{-1} \text{Mpc}^{-1} \quad (6)$$

$$\Omega_m = 1.0132 - 0.00710 \frac{r_{pf}}{\alpha} (\pm 0.0032), \quad (7)$$

where the units of r_{pf} are h^{-1} Mpc . Deviations are indicated for the fit lines from the data points used to derive them. Expressions that relate Ω_m and H_0 are readily obtained from the equation pairs (4), (5), and (6), (7),

$$H_0 + 76.78\Omega_m = 91.47, \quad k^* = 0.3 \text{ } h \text{ } \text{Mpc}^{-1}, \quad (8)$$

and

$$H_0 + 76.80\Omega_m = 91.43, \quad k^* = 0.15 \text{ } h \text{ } \text{Mpc}^{-1}. \quad (9)$$

The agreement between Equations (8) and (9) gives an indication that the variation in r_p magnitude as a function of k^* is not a major problem.

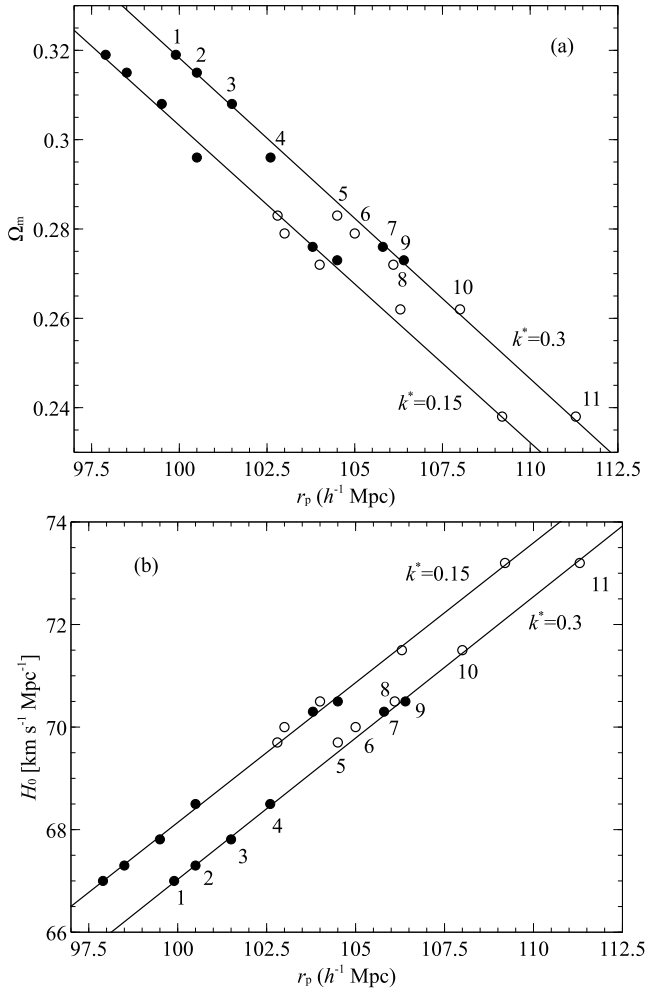


FIG. 4.— Ω_m and H_0 values as a function of $\xi(r)$ peak locations. These values and the parameter sets used to compute $\xi(r)$ were acquired from the following references: (1) Calabrese et al. (2017) (*Planck*), (2) *Planck* 2013 results XVI (2014), (3) *Planck* 2015 results XIII (2016), (4) Calabrese et al. (2017) (*WMAP9+ACT*), (5) Calabrese et al. (2013) (*WMAP9+ACT*), (6) Hinshaw et al. (2013) (*WMAP9*), (7) Calabrese et al. (2017) (*WMAP9+eCMB*), (8) Hinshaw et al. (2013) (*WMAP+eCMB*), (9) Calabrese et al. (2017) (*WMAP+SPT*), (10) Calabrese et al. (2013) (*WMAP+SPT*), (11) Spergel et al. (2007) (*WMAP3*). Data sets 1-4 and 7 and 9 incorporated a total neutrino mass of 0.06 eV and were used to derive the fit lines. The filled in circles indicate those data points. The other data sets assigned a neutrino mass value of zero. The fit line formulas are for (a) $\Omega_m = 1.0363 - 0.00718r_p$, $k^* = 0.3 h \text{ Mpc}^{-1}$ and $\Omega_m = 1.0132 - 0.00710r_p$, $k^* = 0.15 h \text{ Mpc}^{-1}$ and for (b) $H_0 = 11.8994 + 0.5513r_p$ $\text{km s}^{-1}\text{Mpc}^{-1}$, $k^* = 0.3 h \text{ Mpc}^{-1}$ and $H_0 = 13.6095 + 0.5453r_p$ $\text{km s}^{-1}\text{Mpc}^{-1}$, $k^* = 0.15 h \text{ Mpc}^{-1}$.

We have referred to the near degeneracy of the Ω_m , H_0 pair in CMB parameter evaluations. Figures 1 and 4, as well as Equations (8) and (9) demonstrate an inverse relationship between the pair components for various CMB compatible data sets and fits, but do not unambiguously demonstrate a degeneracy. That degeneracy shows up most vividly when varying the parameters for a specific data set to obtain an optimum fit to a CMB TT power spectrum. Percival et al. (2002) demonstrated that the degeneracy is well approximated by an expression, $\Omega_m h^3 = \text{constant}$. *Planck* 2013 results XVI (2014), sets that constant for their data at 0.0959 ± 0.0006 . Their

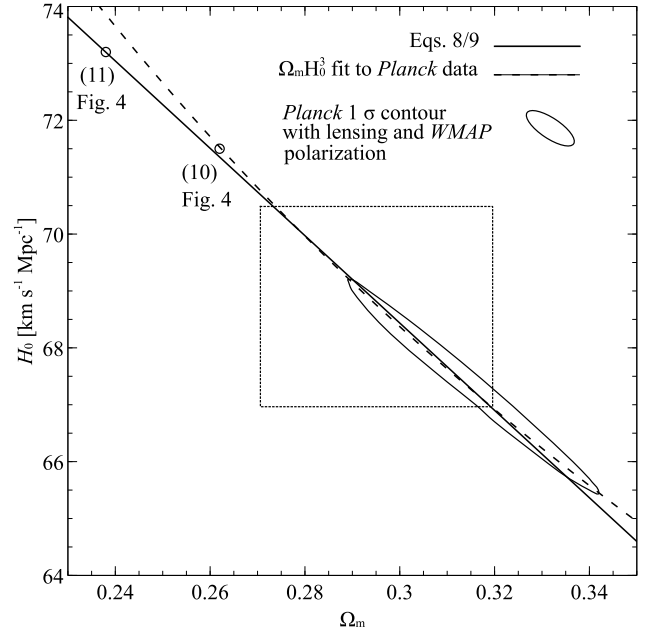


FIG. 5.— Ω_m , H_0 degeneracy as described by Equations 8/9 and compared with the $\Omega_m h^3$ fit to *Planck* 2013 results XVI (2014). Also depicted is the 1σ contour adapted from figure 3 of *Planck* 2013 results XVI (2014), in which the *Planck* data is constrained by the introduction of lensing and *WMAP* polarization. The rectangle indicates the bounds within which Equations 8 and 9 are applicable. Within those bounds the agreement with the degeneracy relationship described by *Planck* 2013 results XVI (2014) is excellent. Nine of the eleven Ω_m , H_0 pairs plotted in Figure 4 fall within the bounded area. The two that fall outside, (10) and (11) are plotted here, and as indicated on Figure 4, also fall on or near the Equations 8/9 fit line.

figure 3, provides an Ω_m , H_0 degeneracy plot for which the spectral index, n_s has been varied to maintain a good fit to the characteristic TT spectrum curve (i.e., Figure 1a). Figure 5 compares the *Planck* results with the Ω_m , H_0 relationship described by Equations (8) and (9) and finds excellent agreement over the applicable range of those equations.

What is most germane to this discussion is that while there is difficulty in arriving at a specific pair of Ω_m , H_0 values from CMB measurements, Figures 2 and 4 indicate that the same is not true for 2PCF measurements. The different CMB compatible solutions are clearly defined by differences in their r_p values. Equations (4) through (7) and Figure 4 map the Ω_m , H_0 values as a function of r_p . In the following section we use that mapping in conjunction with the results of the 2PCF BAO study r_p determinations to break the CMB Ω_m , H_0 degeneracy.

3. ISOTROPIC BAO STUDIES

Table 2 lists a number of isotropic BAO studies. The listings are not comprehensive, but are representative and include early pioneering work and major studies conducted since that early work. Several studies employed the modified matter power spectrum directly (Cole et al. 2005; Percival et al. 2007, 2010; Blake et al. 2011a). We focus on the 2PCF analyses. Table 2 entries from Padmanabhan et al. (2012), and after, employed the reconstruction technique instituted by Eisenstein et al. (2007a), which uses the galaxy density data to assess the velocity field and then, in essence, runs the clock back-

TABLE 2
REPRESENTATIVE ISOTROPIC BAO STUDIES.

| Ref. | # galaxies | Eff. z | BAO study derived Ω_m | Concurrent CMB ^a | Fid. Cosmol. $\Omega_m, \Omega_b h^2, h_0, n_s$ | α |
|------|--------------|-----------------|------------------------------|-----------------------------|---|---------------------|
| 1 | 46 748 | 0.35 | 0.273 ± 0.025 | <i>WMAP1</i> | 0.3, 0.024 0.7, 0.98 | 1.03 ± 0.05^b |
| 2 | 221 414 | < 0.3 | 0.231 ± 0.021 | <i>WMAP1</i> | | |
| 3 | 522 280 | | $0.256^{+0.029}_{-0.024}$ | <i>WMAP3</i> | | |
| 4 | 895 834 | 0.275 | 0.286 ± 0.018 | <i>WMAP5</i> | | |
| 5 | 152 117 | $0.1 < z < 0.9$ | 0.27 | <i>WMAP5</i> | | |
| 6 | 75 117 | 0.106 | – | <i>WMAP7</i> | 0.27, 0.02227, 0.7, 0.966 | 1.039 ± 0.062 |
| 7 | 132 509 | 0.6 | – | <i>WMAP7</i> | 0.27, 0.0226, 0.71, 0.96 | 1.075 ± 0.055 |
| 8 | 105 831 | 0.35 | 0.280 ± 0.014^c | <i>WMAP7</i> | 0.274, 0.0225, 0.702, 0.968 ^c | 1.012 ± 0.019 |
| 9 | 264 283 | 0.57 | – | <i>WMAP7</i> | 0.274, 0.0224, 0.7, 0.95 | 1.024 ± 0.016 |
| 10 | 690 826 DR11 | 0.57 | – | <i>Planck13</i> | 0.274, 0.0224, 0.7, 0.95 | 1.0178 ± 0.0089 |
| 11 | 158 741 | 0.44^d | – | <i>Planck13</i> | 0.27, 0.0226, 0.71, 0.96 | 1.061 (4.8%) |
| | | 0.73 | | | | 1.03 (3.4%) |
| 12 | 361 762 | 0.32 | – | <i>Planck15</i> | 0.29, 0.0225, 0.7, 0.97 | 1.0251 ± 0.0169 |
| | DR12 LOWZ | | | | | |
| | 777 202 | 0.57 | | | | 1.0064 ± 0.0096 |
| | DR12 CMASS | | | | | |

a) CMB Ω_m values: *WMAP1*=0.27, *WMAP3*= 0.238, *WMAP5*=0.273, *WMAP7*=0.272, *Planck13*=0.315, *Planck15*=0.308. See NASA’s online utility at <http://lambda.gsfc.nasa.gov>. for links to appropriate references.

b) Value of α extracted from Eisenstein et al. (2005) fig. 6. The ± 0.05 error approximates the precision of the study.

c) Found in companion paper, Mehta et al. (2012).

d) Kazin et al. (2014) evaluated α at three effective redshifts. However, the dataset for effective $z = 0.60$ is a composite of data points and mock catalogues from effective $z = 0.44$ and 0.73 and has been omitted to avoid the inclusion of correlated data sets.

Note. – This table includes both studies that employed the modified matter power spectrum and those that drew upon its Fourier transform, the 2PCF. Derived values of Ω_m in column 4 are only shown for those papers that explicitly identified them in their abstract. Padmanabhan et al. (2012) (reference 8) was first to exploit the reconstruction technique of Eisenstein et al. (2007b) and all papers listed in the table after Padmanabhan et al. (2012) also employed reconstruction. In all those instances the value recorded for α is post-reconstruction.

References. (1) Eisenstein et al. (2005); (2) Cole et al. (2005); (3) Percival et al. (2007); (4) Percival et al. (2010); (5) Blake et al. (2011a); (6) Beutler et al. (2011); (7) Blake et al. (2011b); (8) Padmanabhan et al. (2012); (9) Anderson et al. (2012); (10) Anderson et al. (2014); (11) Kazin et al. (2014); (12) Cuesta et al. (2016)

wards and reverses the inflowing mass. That procedure goes far to ameliorate the effects of non-linearities.

Table 3 assembles the studies with entries in the last two columns of Table 2. We use the stated fiducial cosmology to obtain r_{pf} for each of the listed studies, for both $k^* = 0.15$ and $0.3 h \text{ Mpc}^{-1}$, employing Equation (3). We further use those results and the BAO study derived α values in Equations (4) through (7) to compute CMB compatible values of Ω_m and H_0 . We have performed our computations in real space, while a number of the studies listed in Tables 2 and 3 worked in redshift space. For a monopole/isotropic analysis, the difference in the two lies in multiplication by the Kaiser factor, $\xi_s = (1 + \frac{2}{3}\beta + \frac{1}{5}\beta^2)\xi_r$, where β is a redshift distortion factor (Kaiser 1987; Hamilton 1992). Again, we do not expect significant change in the factor over the small range of the BAO feature shift and hence the peak location differences in real and redshift space are identical. The fiducial cosmology may not be CMB compatible, e.g., the combination $\Omega_m = 0.3$ and $H_0 = 0.7$ was once a popular choice and was used in Eisenstein et al. (2005). A quick check, using Equation (8) or (9) reveals that either Ω_m or H_0 is too high for this combination to satisfy CMB observations. Regardless of whether or not the fiducial cosmology is consistent with CMB observations, we expect, and assume, that the data derived outcomes are.

The standard deviations in Table 3 stem directly from those of the α ’s (see Table 2) provided by the various

studies. We have further added in quadrature the deviation of the appropriate fit line to each of the Table 3 uncertainties, although the fit line deviations are small enough to have a negligible effect. The results are in reasonable agreement with one another. Out of a total of 10 data sets, within 8 separate studies, the lowest Ω_m mean is 0.287 ± 0.014 (Padmanabhan et al. 2012) and 0.287 ± 0.008 (Cuesta et al. 2016) and the highest is 0.325 ± 0.037 (Blake et al. 2011b). The corresponding extremes for H_0 are $66.52 \pm 2.80 \text{ km s}^{-1} \text{ Mpc}^{-1}$ (Blake et al. 2011b) and 69.38 ± 1.05 (Padmanabhan et al. 2012) and $69.36 \pm 0.54 \text{ km s}^{-1} \text{ Mpc}^{-1}$ (Cuesta et al. 2016).

Though the same galaxy surveys, or expanded versions, have been used in some of the investigations, taking into account the use of different mock catalogue ensembles, each of the data sets is independent and identically distributed and we compute weighted means and weighted standard deviations accordingly. For $\bar{\Omega}_{mw}$ and $\bar{\sigma}_{mw}^2$:

$$\bar{\Omega}_{mw} = \frac{\sum_{i=1}^N \Omega_{mi} / \sigma_{mi}^2}{\sum_{i=1}^N 1 / \sigma_{mi}^2}, \quad (10)$$

² See NIST Dataplot at: <http://www.itl.nist.gov/div898/software/dataplot/homepage.htm> and search under “weighted mean” and “weighted standard deviation”. $w_{mi} \equiv 1/\sigma_{mi}^2$.

TABLE 3
 BAO STUDIES FROM TABLE 2 WITH ENTRIES OF α IN THE LAST COLUMN

| Ref. | $k^* = 0.3$ | | $k^* = 0.15$ | |
|------------------|-------------|---------------------------|--------------|---------------------------|
| | r_{pf} | Ω_m H_0 | r_{pf} | Ω_m H_0 |
| 1 | 104.0 | 0.311±0.037 67.57±2.82 | 102.8 | 0.305±0.036 68.03±2.76 |
| 2 | 105.5 | 0.307±0.044 67.88±3.35 | 103.2 | 0.308±0.042 67.77±3.25 |
| 3 | 106.5 | 0.325±0.037 66.52±2.80 | 104.6 | 0.322±0.036 66.67±2.72 |
| 4 | 105.5 | 0.288±0.014 69.37±1.08 | 103.5 | 0.287±0.014 69.38±1.05 |
| 5 | 104.9 | 0.301±0.012 68.38±0.89 | 102.5 | 0.302±0.012 68.19±0.86 |
| 6 | 104.9 | 0.296±0.007 68.72±0.50 | 102.5 | 0.298±0.007 68.53±0.49 |
| 7 ($z = 0.44$) | 106.5 | 0.316±0.035 67.24±2.67 | 104.6 | 0.313±0.034 67.37±2.59 |
| ($z = 0.73$) | 106.5 | 0.294±0.025 68.90±1.94 | 104.6 | 0.292±0.025 68.99±1.89 |
| 8 ($z = 0.32$) | 104.5 | 0.304±0.012 68.10±0.93 | 102.9 | 0.300±0.012 68.35±0.91 |
| ($z = 0.57$) | 104.5 | 0.291±0.008 69.14±0.55 | 102.9 | 0.287±0.008 69.36±0.54 |
| Weighted totals | | 0.296±0.007 68.73±0.52 | | 0.296±0.008 68.74±0.57 |

NOTE. — r_{pf} was computed for each of the studies using the fiducial cosmology parameters listed in Table 2. H_0 units are $\text{km s}^{-1} \text{Mpc}^{-1}$, r_{pf} units are $h^{-1} \text{Mpc}$.

REFERENCES. — (1) Eisenstein et al. (2005); (2) Beutler et al. (2011); (3) Blake et al. (2011b); (4) Padmanabhan et al. (2012); (5) Anderson et al. (2012); (6) Anderson et al. (2014); (7) Kazin et al. (2014); (8) Cuesta et al. (2016)

$$\bar{\sigma}_{mw} = \frac{\left(\sum_{i=1}^N (\Omega_{mi} - \bar{\Omega}_{mw})^2 / \sigma_{mi}^2 \right)^{1/2}}{\left((N-1)/N \sum_{i=1}^N 1/\sigma_{mi}^2 \right)^{1/2}} \quad (11)$$

and similarly for \bar{H}_{0w} and $\bar{\sigma}_{H_0w}$. The weighted totals, given in Table 3, are $\bar{\Omega}_{mw} = 0.296 \pm 0.007$, $\bar{H}_{0w} = 68.73 \pm 0.52 \text{ km s}^{-1} \text{Mpc}^{-1}$ for $k^* = 0.3 h \text{ Mpc}^{-1}$ computations and 0.296 ± 0.008 and $68.74 \pm 0.57 \text{ km s}^{-1} \text{Mpc}^{-1}$ for $k^* = 0.15 h \text{ Mpc}^{-1}$ computations. We immediately conclude that the variation of r_p as a function of k^* has no effect on the results. We have had to display four significant figures for the \bar{H}_{0w} results to demonstrate the slightest difference. The weighted means are dominated by the Padmanabhan et al. (2012); Anderson et al. (2012, 2014); Cuesta et al. (2016) measurements. The small weighted standard deviation values can be attributed to the narrow spread of individual mean values (Ω_{mi} , H_{0i}) between the studies, the tight uncertainties in the dominant studies, and to the weighting of multiple surveys. The results are in excellent agreement with the SNe Ia Ω_m value of 0.295 ± 0.034 (Betoule et al. 2014) and with the *WMAP9* + *ACT* value of 0.296 ± 0.025 (Calabrese et al. 2017). They are also in line with *Planck* 2015 results XIII (2016) at 0.308 ± 0.012 , but are at greater variance with the Calabrese et al. (2017), *Planck*, value of 0.319 ± 0.013 .

We have tested perturbing the derived $\bar{\Omega}_{mw}$ and \bar{H}_{0w} quantities by varying w from -1.02 to -0.98 and Ω_K from

 TABLE 4
 COMPARISON OF r_d AND r_p

| h | 0.670 | 0.685 | 0.703 | 0.705 |
|-------------|--------|--------|--------|--------|
| Ω_m | 0.319 | 0.296 | 0.276 | 0.273 |
| r_p (Mpc) | 149.10 | 149.78 | 150.50 | 150.92 |
| r_d (Mpc) | 147.15 | 148.18 | 148.79 | 149.23 |
| r_p/r_d | 1.013 | 1.011 | 1.011 | 1.011 |

NOTE. — The values of r_p and r_d and their ratio are provided for parameter sets taken from Table 1, r_p computed with $k^* = 0.3 h \text{ Mpc}^{-1}$. The CMB data compatible cosmologies are here represented by their values of h and Ω_m . We use units $h^{-1} \text{Mpc}$ or Mpc for r_d and r_p . The units are specifically spelled out in each instance.

-0.003 to 0.003. We proceeded by generating a Fourier transform of the modified matter power spectrum using the weighted quantities as input parameters. The flat, $w = -1$, solution falls within the computed deviations of the fit-lines [Equations (4) through (7)]. For reference, with $k^* = 0.3 h \text{ Mpc}^{-1}$, $r_p = 102.7 h^{-1} \text{Mpc}$. That is in comparison to a value of $102.6 h^{-1} \text{Mpc}$ for the Calabrese et al. (2017) *WMAP9*+*ACT* fit with which the derived weighted parameters are closely aligned. We found shifts in that computed r_p position, which vary within $\sim \pm 0.1$ per cent for the w differentials and within $\sim \pm 0.4$ per cent for the Ω_K deltas. For the w deviations those shifts translate to less than a few tenths of a per cent change in Ω_m , and negligible changes in H_0 . The introduction of curvature altered the Ω_m value by up to a per cent, and that of H_0 by less than 0.3 per cent.

4. DEMONSTRATION THAT $D_V(z)/r_d \neq \alpha D_{Vf}(z)/r_{df}$

Taking the inequality in the section heading and introducing a dummy parameter, $\gamma(z)$, permits writing an equality and avoids cumbersome referrals:

$$\gamma(z) \frac{D_V(z)}{r_d} = \alpha \frac{D_{Vf}(z)}{r_{df}} \quad (12)$$

Though Eisenstein et al. (2005) defined $D_V(z)$, they made no statement regarding Equation (12), $\gamma(z) = 1$. The origins of a variant of that equation can be found in their figure 6 which plots χ^2 versus scale change (α) where scale change is altered by varying $D_V(z)$. What was required was a monotonic variation of scale change with $D_V(z)$. Succeeding teams (Sánchez et al. 2009; Kazin et al. 2010; Beutler et al. 2011) assumed that the variation was linear, i.e., $\alpha = D_V(z)/D_{Vf}(z)$. The introduction of Equation (12), $\gamma(z) = 1$, followed shortly after and has become standard (Padmanabhan et al. 2012; Mehta et al. 2012; Anderson et al. 2012, 2014; Kazin et al. 2014; Aubourg et al. 2015; Cuesta et al. 2016), but with either no attribution or an incorrect attribution to Eisenstein et al. (2005). To investigate the validity of this form we rearrange Equation (12) as follows:

$$\gamma(z) \frac{D_V(z)}{D_{Vf}(z)} = \alpha \frac{r_d}{r_{df}}, \quad (13)$$

and immediately observe that the lefthand side of Equation (13) is dependent upon z . On the righthand side, r_d and r_{df} are dependent only upon their particular cosmologies. Also, recall that $\alpha \equiv r_{pf}/r_p$. We have probed the values of r_p over the range of CMB compatible cosmologies considered in this paper and at z values appraised in various isotropic studies from 0.1 to 0.73, and

for each cosmology find no change in r_p as a function of z . Thus the righthand side of equation (13) is independent of z .

While r_d can be computed using CAMB, here, we reproduce a fitting formula furnished by Aubourg et al. (2015) that gives a close approximation to the CAMB values, accurate to 0.021 per cent with values of ω_b and ω_{cb} within 3σ of the *Planck* derived values:

$$r_d \simeq \frac{55.154 \exp[-72.3(\omega_\nu + 0.0006)^2]}{\omega_{cb}^{0.25351} \omega_b^{0.12807}} \text{ Mpc}, \quad (14)$$

where $\omega_x \equiv \Omega_x h^2$ and the subscript, *cb*, refers to the combined mass fraction of baryons and CDM. In Table 4 the values of r_p and r_d are compared using four of the cosmologies from Table 1 and r_p is found to be about 1 per cent higher than r_d throughout the range (for $k^* = 0.3 h \text{ Mpc}^{-1}$).

From what was just stated it is clear that the righthand side of equation (13) is very close to unity. If, for example, we take a fiducial cosmology with $\Omega_m = 0.276$ and a data cosmology with $\Omega_m = 0.319$ from Table 4, then the righthand side of equation (13) is equal to 0.998. Thus, for $\gamma(z) = 1$ we are left with the suspicious result that regardless of cosmology or redshift, $D_V(z)$ is nearly identical to $D_{Vf}(z)$. This observation should suffice to discredit equation (12) with $\gamma(z) = 1$. However, since the equation is so firmly entrenched in the literature, it behooves us to go further and investigate whether or not it is at least approximately correct. Using Equation 1, we perform calculations for a flat cosmology and with $w = -1$ in which instance:

$$H(z) = H_0[\Omega_m(1+z)^3 + 1 - \Omega_m]^{1/2}. \quad (15)$$

Values for D_M are obtained from the Wright (2006) online calculator³.

Looking at the ratio of $D_V(z)/D_{Vf}(z)$ on the lefthand side of Equation (13), if that ratio differs substantially from unity and/or varies with z then $\gamma(z) \neq 1$ and the proof of inequality would be established. Variation of $D_V(z)/D_{Vf}(z)$ as a function of z would further establish that $\alpha \neq D_V(z)/D_{Vf}(z)$. The results for the ratio of $D_V(z)/D_{Vf}(z)$ are plotted in Figure 6, where we see a variation as a function of redshift and divergence from Equation (13), $\gamma(z) = 1$, throughout. When the precision of BAO studies was 3 to 4 per cent, Equation (12), $\gamma(z)=1$, was at best a poor approximation. Considering that BAO studies have now attained a one per cent level of precision and that future studies aim for sub per cent levels of precision, the continued use of Equation (12), $\gamma(z) = 1$, cannot be justified.

5. CONCLUSIONS

BAO studies each represent an enormous effort, starting with the underlying spectroscopic galactic survey, and continuing with the appropriate grooming and masking of the survey results, the production of hundreds to upwards of over a thousand mock catalogues, and the substantial computation investment devoted to extricating the correlation function. For 2PCF analysis, indisputably, the gem that is ultimately extracted from the reams of data is the BAO feature shift-parameter, α .

³ <http://www.astro.ucla.edu/%7Ewright/ACC.html>

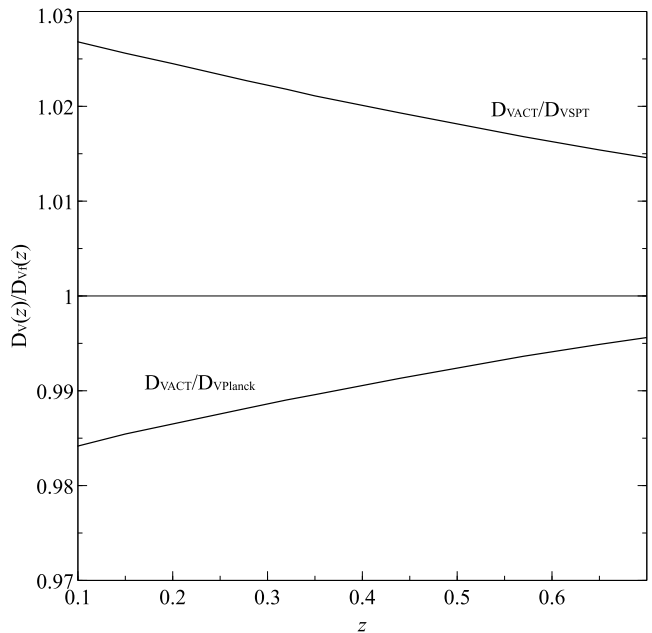


FIG. 6.— $D_V(z)/D_{Vf}(z)$ as a function of redshift, where the Calabrese et al. (2017) *WMAP+ACT* data is used to calculate D_V and the Calabrese et al. (2017) *WMAP+SPT* data and the Calabrese et al. (2017) (*Planck*) data are used to calculate two different fiducial values, D_{Vf} . See Table 1 for specific parameter values.

Application of the shift-parameter to evaluating the cosmological quantities Ω_m and H_0 is a central aspect of this work. The following assumptions and steps lead up to that application:

1. Assumption of a CMB compatible cosmology based on Λ CDM with $\Omega_K \simeq 0$ and $w \simeq -1$.
2. Perturbations such as galactic bias affect the absolute position of the correlation function peak. We take the magnitude of these perturbations as constant over the short range defined by α .
3. That resistance of the peak shift differential to perturbation enables us to perform our calculations using a basic format for analyzing the 2PCF studies, a Fourier transform of the matter power spectrum that has been modified by inclusion of the Eisenstein & Hu (1998a, 1999) no-wiggle term. The modified matter power spectrum employs a damping factor, k^* , which, dependent upon its magnitude, yields dissimilar values of r_p . We purposefully selected two values of k^* that gave sizably different peak locations. Yet, computations performed with both produced near identical results.
4. The Fourier transform of the modified matter spectrum is applied to a series of CMB compatible parameter sets. Both components of the Ω_m, H_0 pair are mapped as a function of r_p , and fit lines obtained. Here we emphasize that though the Ω_m, H_0 pair is near degenerate when fitting CMB TT spectra, specific pair values are clearly resolved when mapped against r_p .
5. At this point we turn to the BAO studies and apply the Fourier transform of the modified matter spec-

trum to their fiducial cosmologies, deriving r_{pf} for each study.

- Finally, the BAO study derived values of α are used to obtain r_p , and in turn, values of Ω_m and H_0 from the CMB compatible fit lines.

Despite the effort that has gone into attaining precise values of α , its past application is suspect, as delineated in Section 4 where we have demonstrated that a formulation in widespread use, relating the parameters D_V , D_{Vf} , r_d , r_{df} and α in a single equation is incorrect. On the other hand, the substance of those past studies is comprised of high quality 2PCF isotropic BAO data sets. The 10 data sets analyzed herein, found in 8 different studies, demonstrate impressive consistency. The weighted means and standard deviations of Ω_m and H_0 derived from these studies are $\bar{\Omega}_{mw} = 0.296 \pm 0.008$, and $\bar{H}_{0w} = 68.7 \pm 0.55 \text{ km s}^{-1} \text{ Mpc}^{-1}$.

These results are in close agreement with conclusions reached in the SNe Ia (Betoule et al. 2014) investigation and the *WMAP9+ACT* (Calabrese et al. 2017) computation. Through the consistency between the different data sets, the small deviations of the dominant studies, and the weighting of multiple studies, the precision rivals that of *Planck* 2015 results XIII (2016). We are quick to add that this consequence has come about through an amalgam of the BAO and CMB disciplines. Of particular note, though the weighted parameter outcomes depend on the fit-lines derived from CMB studies, they are dissociated from specific CMB results.

We acknowledge the use of the Legacy Archive for Microwave Background Data Analysis (LAMBDA), part of the High Energy Astrophysics Science Archive Center (HEASARC). HEASARC/LAMBDA is a service of the Astrophysics Science Division at the NASA Goddard Space Flight Center.

REFERENCES

- Alam S., Ata M., Bailey S., et al., 2016, preprint (arXiv:1607.03155)
- Anderson L., Aubourg E., Bailey S., et al., 2012, MNRAS, 427, 3435
- Anderson L., Aubourg E., Bailey S., et al., 2014, MNRAS, 441, 24
- Aubourg E., Bailey S., Bautista J.E., et al., 2015, Phys. Rev. D, 92, 123516
- Bassett B., & Hlozek R., 2010, in Dark Energy: Observational and Theoretical Approach, ed., P. Ruiz-Lapuente, (Cambridge: Cambridge Univ. Press), 246
- Betoule M., Kessler R., Guy J., et al., 2014, A&A, 568, A22
- Beutler F., Blake C., Colless M., et al., 2011, MNRAS, 416, 3017
- Blake C., Brough S., Colless M., et al., 2011a, MNRAS, 415, 2876
- Blake C., Davis T., Poole, G.B., et al., 2011b, MNRAS, 415, 2892
- Bolejko K., C el erier M.-N., & Krasiński A., 2011, CQGra, 28, 16
- Calabrese E., Hlozek R.A., Battaglia N., et al., 2013, Phys. Rev. D, 87, 103012
- Calabrese E., Hlozek R.A., Bond R., et al., 2017, Phys. Rev. D, 95, 063525
- Clarkson C., 2012, CRPhy, 13, 682
- Cole S., Percival W.J., Peacock J.A., et al., 2005, MNRAS, 362, 505
- Colless M., Peterson B.A., Jackson C., et al., 2003, preprint (arXiv:astro-ph/0306581)
- Crocce M., & Scoccimarro R., 2008, Phys. Rev. D, 77, 023533
- Cuesta A.J., Vargas-Magaña M., Beutler F., et al., 2016, MNRAS, 457, 1770
- Das S., Louis T., Nolta M.R., et al., 2014, JCAP, 4, 14
- Drinkwater M.J., Jurek R.J., Blake C., et al., 2010, MNRAS, 401, 1429
- Dunkley J., Calabrese E., Sievers J., et al., 2013, JCAP, 7, 25
- Eisenstein D.J., & Hu W., 1998a, ApJ, 496, 605
- Eisenstein D.J., Hu W., & Tegmark M., 1998b, ApJ, 504, L57
- Eisenstein D.J., & Hu W., 1999, ApJ, 511, 5
- Eisenstein D.J., Zehavi I., Hogg D., et al., 2005, ApJ, 633, 560
- Eisenstein D.J., Seo H.-J., Sirko E., & Spergel D.N., 2007a, ApJ, 664, 675
- Eisenstein D.J., Seo H.-J., & White M., 2007b, ApJ, 664, 660
- Freedman W.L., Madore B.F., Scowcroft V., et al., 2012, ApJ, 758, 24
- George E.M., Reichardt C.L., Aird K.A., et al., 2015, ApJ, 799, 177
- Guzik J., Bernstein G., & Smith R. E., 2007, MNRAS, 375, 1329
- Hamilton A.J.S., 1992, ApJ, 385, L5
- Hinshaw G., Larson D., Komatsu E., et al., 2013, ApJS, 208, 19
- Hu W., & Dodelson S., 2002, ARA&A, 40, 171
- Hubble E., 1929, Proc. Natl. Acad. Sci. USA, 15, 168
- Kaiser N., 1987, MNRAS, 227, 1
- Kazin E.A., Blanton M.R., Scoccimarro R., et al., 2010, ApJ, 710, 1444
- Kazin E.A., Koda J., Blake C., et al., 2014, MNRAS, 441, 3524
- Lewis A., Challinor A., & Lasenby A., 2000, ApJ, 538, 473
- Mehta K.T., Cuesta A.J., Xu X., Eisenstein D.J., & Padmanabhan N., 2012, MNRAS, 427, 2168
- Padmanabhan N., Xu X., Eisenstein D.J., et al., 2012, MNRAS, 427, 2132
- Peebles P.J.E., & Yu J.T., 1970, ApJ, 162, 815
- Percival W.J., Sutherland W., Peacock J.A., et al., 2002, MNRAS, 337, 1068
- Percival W.J., Nichol R.C., Eisenstein D.J., et al., 2007, ApJ, 657, 51
- Percival W.J., Reid B.A., Eisenstein D.J., et al., 2010, MNRAS, 401, 2148
- Perlmutter S., Aldering G., Goldhaber G., et al., 1999, ApJ, 517, 565
- Planck* 2013 results XVI, 2014, A&A, 571, A16
- Planck* 2015 results XI, 2016, A&A, 594, A11
- Planck* 2015 results XIII, 2016, A&A, 594, A13
- Planck* intermediate results XLVI, 2016, A&A, 596, A107
- Reid B., Ho S., Padmanabhan N., et al., 2016, MNRAS, 455, 1553
- Riess A.G., Filippenko V., Challis P., et al., 1998, AJ, 116, 1009
- Riess A.G., Macri L., Casertano S., et al., 2011, ApJ, 730, 119
- Riess A.G., Macri L.M., Hoffmann S.L., et al., 2016, ApJ, 826, 56
- S anchez A.G., Baugh C.M., & Angulo R., 2008, MNRAS, 390, 1470
- S anchez A.G., Crocce M., Cabre A., Baugh C.M., & Gazta naga E., 2009, MNRAS, 400, 1643
- Seo H.-J., & Eisenstein D.J., 2003, ApJ, 598, 720
- Silk J., 1968, ApJ, 151, 459
- Smith R.E., Scoccimarro R., & Sheth R.K., 2008, Phys. Rev. D, 77, 043525
- Spergel D.N., Bean R., Dore O., et al., 2007, ApJ, 170, 377
- Story K.T., Reichardt C.L., Hou Z., et al., 2013, ApJ, 779, 86
- Suzuki N., Rubin D., Lidman C., et al., 2012, ApJ, 746, 85
- Weinberg D.H., Mortonson M.J., Eisenstein D., et al., 2013, PhR., 530, 2, 87
- Wright E.L., 2006, PASP, 118, 1711
- York D.G., Adelman J., Anderson Jr. J.E., et al., 2000, AJ, 120, 1579